ALEXANDER LAVROV*

THEORETICAL INVESTIGATION OF THE KAISER EFFECT MANIFESTATION IN ROCKS AFTER TRUE TRIAXIAL PRE-LOADING

TEORETYCZNE BADANIA EFEKTU KAISERA W SKAŁACH PODDANYCH RZECZYWISTEMU TRÓJOSIOWEMU OBCIĄŻENIU WSTĘPNEMU

Kaiser effect takes place in rocks when they are cyclically loaded with the peak stress magnitude increasing from cycle to cycle. The effect consists in non-reprodicibility of acoustic emission activity at stress values lesser than the maximum previously applied ("memorized") stress. As soon as this "memorized" stress level is attained, acoustic emission activity increases dramatically. It allows to estimate the pre-stress level relatively simply. For practical application of the Kaiser effect to geo-stress measurements, it is necessary to know its features in rock samples which were under triaxial state of stress *in situ*. So far, all experimental and theoretical investigations of the Kaiser effect have been limited to the cases of uniaxial or axisymmetric triaxial pre-loading ($\sigma_1 > \sigma_2 = \sigma_3$). Here, the first attempt is made to study the Kaiser effect in rock samples which were under true triaxial stress state in situ ($\sigma_1 > \sigma_2 > \sigma_3$).

The behaviour of a rock sample containing 1000 arbitrarily oriented penny-shaped cracks was stimulated. The rock sample was "loaded" in two cycles. The first cycle was true triaxial compression with maximum principal stresses different from each other: $\sigma_1^I > \sigma_2^I > \sigma_3^I$. The second cycle was a uniaxial compressive test as it is normally carried out on rock samples extracted from the rock mass. During this test, the samples was "loaded" in the direction of the first-cycle σ_1^I-axis. As a result, curves "acoustic emission activity versus stress" were obtained for the second-cycle loading for various combinations of the first-cycle principal stresses.

Processing AE curves has shown that the Kaiser effect manifestation in rock samples, previously subjected to true triaxial *in situ* stress state, is far more complex than in the samples after axisymmetric triaxial pre-loading. In the former, the Kaiser effect is lesser distinct, the AE begins to increase from the beginning of the uniaxial loading and

* KATHOLIEKE UNIVERSITEIT LEUVEN, FACULTY OF APPLIED SCIENCE, DEPARTMENT OF CIVIL ENGINEERING, MINING DIVISION, W. DE CROYLAAN 2, B-3001 HEVERLEE, BELGIUM

continues to rise to $\sigma_1 = \sigma_1^1 - (k+1)\sigma_3^1$, and a sharp increase in AE activity is not observed. From the shape of the AE curve only, it is hardly possible to conclude about the type of the in situ stress state and to estimate absolute values of in situ principal sresses. The intermediate and the minimum in situ principal stresses have a pronounced influence on the shape of the AE curve and on the Kaiser effect stress value. This and other results of thw simulation are to be always taken into account when using the Kaiser effect for stress measurement in rocks.

Key words: Kaiser effect, stress measurement, true triaxial stress state, acoustic emission, microcracks, numerical simulation.

Efekt Kaisera występuje w skałach obciążonych cyklicznie z wielkością maksymalnego naprężenia rosnącego z każdym cyklem. Efekt ten polega na braku odtwarzalności działania emisji akustycznej przy wartości naprężenia mniejszej od maksymalnej wartości uprzednio przyłożonego („zapamiętanego") naprężenia. Skoro tylko ten „zapamiętany" poziom naprężenia zostaje osiągnięty, działanie emisji akustycznej dramatycznie wzrasta. Pozwala to stosunkowo łatwo ocenić poziom wcześniej występującego naprężenia. Dla celów praktycznego zastosowania efektu Kaisera w pomiarach geo-naprężeń konieczna jest znajomość tego zjawiska w próbkach skał poddanych trójosiowemu naprężeniu *in situ*.

Dotychczasowe eksperymentalne i teoretyczne badania efektu Kaisera ograniczone były do przypadków jednoosiowego lub osiowo-symetrycznego trójosiowego obciążenia wstępnego ($\sigma_1 > \sigma_2 = \sigma_3$). W artykule podjęto próbę zbadania efektu Kaisera w próbkach skał w stanie rzeczywistego trójosiowego naprężenia ($\sigma_1 > \sigma_2 > \sigma_3$).

Symulowano zachowanie się próbki skalnej zawierającej 1000 dowolnie ukierunkowanych pęknięć o kształcie eliptycznym. Próbkę skalną obciążano w dwóch cyklach. Pierwszy cykl stanowiło rzeczywiste trójosowe ściskanie przy maksymalnych głównych naprężeniach różnych od siebie: $\sigma_1^1 > \sigma_2^1 > \sigma_3^1$. Drugi cykl stanowiła jednoosiowa próba ściskania, taka jak zwykle przeprowadzana jest na próbkach skał pobranych z górotworu. W trakcie testu próbka była obciążana w kierunku osi σ_1^1 pierwszego cyklu. Jako wynik otrzymano zależność emisji akustycznej AE w funkcji naprężenia dla drugiego cyklu obciążenia w różnych kombinacjach naprężeń głównych z pierwszego cyklu.

Przebieg krzywych emisji akustycznej AE wskazuje, że występowanie efektu Kaisera w próbkach skalnych poddanych uprzednio rzeczywistemu trójosiowemu naprężeniu jest daleko bardziej złożone niż w próbkach po osio-symetrycznym trójosiowym wstępnym obciążeniu. W pierwszym przypadku efekt Kaisera jest mniej wyraźny, krzywa emisji akustycznej AE zaczyna wzrastać od początku jednoosiowego obciążenia i wzrasta do wartości $\sigma_1 = \sigma_1^1 - (k+1)\sigma_3^1$ przy czym nie występuje gwałtowny wzrost emisji akustycznej. Na podstawie tylko kształtu krzywej AE nie można wnioskować o stanie naprężenia *in situ* i oszacować bezwzględne wartości głównych naprężeń *in situ*. Pośrednie i najmniejsze naprężenia głównie *in situ* mają zdecydowany wpływ na kształt krzywej AE i na wartość naprężenia przy którym występuje efekt Kaisera.

Powyższe jak również i inne wyniki symulacji powinny być zawsze brane pod uwagę przy wykorzystaniu efektu Kaisera w pomiarach naprężeń w skałach.

Słowa kluczowe: Efekt Kaisera, pomiar naprężeń, trójosiowy styl naprężenia, emisja akustyczna, mikroszczeliny, symulacja numeryczna.

IMPORTANT NOTATIONS

$\sigma_1,\ \sigma_2,\ \sigma_3$	— *current* values of principal stresses in the first or second loading cycle;
$\sigma_1^I,\ \sigma_2^I,\ \sigma_3^I$	— *peak* values of three principal stresses in the *first* cycle;
σ_{1th}^I	— threshold value of the largest principal stress necessary for the formation of stress memory in the first cycle and, as a consequence, for the appearance of the Kaiser effect in the second cycle. If σ_1^I is lesser than σ_{1th}^I, no stress memory is created in the first cycle;
k	— dimensionless coefficient specific for the rock;
a	— radius of the pre-existing (initial) penny-shaped cracks;
$\alpha_1, \alpha_2, \alpha_3$	— angles between the normal to the plane of a penny-shaped initial crack and the direction of the first-cycle principal stresses;
$\vec{e}_1,\ \vec{e}_2,\ \vec{e}_3$	— unit vectors in the directions of the first-cycle principal stresses;
σ_n	— *current* value of the normal stress acting in the plane of a penny-shaped crack in the first or second cycle;
τ	— *current* value of the shear stress acting in the plane of a penny-shaped crack in the first or second cycle;
σ_n^I	— *peak* value of the normal stress acting in the plane of a penny-shaped crack in the *first* cycle;
τ^I	— *peak* value of the shear stress acting in the plane of a penny-shaped crack in the *first* cycle;
$\vec{e}_\tau^I$	— unit shear vector over the plane of a penny-shaped crack in the *first* cycle;
τ_{eff}	— *current* value of the effective shear stress acting over the plane of a penny-shaped crack in the first or second cycle;
τ_{eff}^I	— *peak* value of the effective shear stress acting over the plane of a penny-shaped crack which was reached in the *first* cycle;
$K_I,\ K_{II},\ K_{III}$	— stress intensity factors of Mode I, Mode II, and Mode III respectively,
K_{Ic}	— the critical value of the Mode I stress intensity factor;
$P',\ P''$	— points on the circulate contour of a penny-shaped crack where tensile cracks (wings) emerge;
l	— *current* length of a tensile crack;
l^I	— *peak* value of the length of a tensile crack reached at the end of the first-cycle loading;
$\vec{e}_\tau^{II}$	— unit shear vector over the plane of a penny-shaped crack in the *second* cycle;
σ_{1*}^{II}	— the value of uniaxial compressive stress at which a tensile crack re-starts growing in the second cycle;
N	— total number of cracks growing at a certain value (loading step) in the second cycle;
σ_{1EK}^{II}	— the value of uniaxial compressive stress at which the Kaiser effect takes place in the second cycle.

1. Introduction

In the recent $10-20$ years the Kaiser effect has been drawing the attention of scientists and researchers in rock mechanics as a possible basis for new stress measurement techniques. The Kaiser effect takes place when rocks and materials are loaded in cyclic regime. The effect consists in the non-reproducibility of acoustic emission (AE) activity of rock at stress values lesser than the peak previously aplied stress level. When the current stress atains this "memorized" stress value, the AE

activity increases suddenly (Kaiser, 1953; Kurita & Fujii, 1979; Yoshikawa & Mogi, 1981; Rzhevskiy et al., 1983; Kuwahara et al., 1990; Li & Nordlund, 1993; Pinińska & Zuberek, 1998). As an appropriate measure of the AE activity, AE count rate (the number of AE pulses collected in 1 sec) is usually used.

The Kaiser effect in such simple and clear form as described above is observed only when the sample is loaded in uniaxial compression. However, when using the Kaiser effect for measurement of geo-stresses, the first cycle is triaxial compression (*in situ*), and the second cycle is uniaxial compression (laboratory test of the core sample extracted from the rock mass). So the stress state types are quite different in the first and the second loading cycles. The Kaiser effect in rock samples after triaxial loading was studied only for the simplest cast of triaxial *axisymmetric* compression in the first cycle: $\sigma_1^I > \sigma_2^I = \sigma_3^I$. Here, Roman numerals in the superscript refer to the number of the loading cycle: the first (I) or the second (II). Inspite of some contradictions in experimental results, the most of research groups have obtained that under triaxial axisymmetric state of stress rocks "memorize" a linear combination of principal stresses given by $\sigma_1^I - (k+1)\sigma_3^I$, where k is a dimensionless coefficient specific for the rock (Holcomb, 1983; Holcomb & Martin, 1985; Hughson & Crawford, 1987; Li & Nordlund, 1993; Shkuratnik & Lavrov, 1997 a; Li, 1998). When being re-loaded in uniaxial compression (second cycle) after this triaxial pre-loading, the rock exhibits the Kaiser effect at the stress value given by:

$$\sigma_1^{II} = \sigma_1^I - (k+1)\sigma_3^I. \tag{1}$$

It can be concluded from expression (1) that no stress memory is formed if σ_1^I is lesser than a certain threshold stress value $\sigma_{1th}^I = (k+1)\sigma_2^I$. This conclusion is in agreement with the experimental fact that rocks do not "memorize" uniform hydrostatic stress state of type $\sigma_1^I = \sigma_2^I = \sigma_3^I$ (Filimonov et al., 2000 b). In this case, σ_1^I is definitively lesser than the threshold stress level σ_{1th}^I since k is positive.

The above experimental results were supported by corresponding two-dimensional (Shkuratnik & Lavrov, 1995; Lavrov, 1998; Li, 1998) and three-dimensional (Lavrov, 1997 a; Shkuratnik & Lavrov, 1998) theoretical models. The models were developed using the concept of rock fracture due to tensile cracks (wings, or kink cracks) generated by pre-existing (initial) shear cracks. Three-dimensional simulation of the Kaiser effect in uniaxially loaded rocks which were previously loaded in triaxial axisymmetric compression has shown that the Kaiser effect stress is indeed given by expression (1) (Lavrov, 1997 a). Within the framework of the theory, k depends on the coefficient of friction between crack faces μ (Lavrov, 1997 a; Li, 1998):

$$k = \frac{2\mu}{\sqrt{1+\mu^2}-\mu}. \tag{2}$$

The Kaiser effect manifestation in a rock sample which was triaxially pre-loaded is far more complex than that in a sample which was pre-loaded uniaxially. In the samples pre-loaded in axisymmetric triaxial conditions, AE begins from the beginning of the loading in the second cycle (uniaxial test), and AE activity rises dramatically when the second-cycle stress approaches the value defined by expression (1). Our recent experiments on rock salt successfully confirmed these results of the earlier simulations (Filimonov et al., 2000 a). Apart from explanation and firm experimental establishment of the Kaiser effect features, this agreement betwen theory and experiment has shown the efficiency and the adequacy of the wing-crack model for description of the Kaiser effect in rocks.

The most interesting and, at the same time, the most difficult for experimental investigation is the Kaiser effect in rocks which were previously under *true* triaxial compression of type $\sigma_1^1 > \sigma_2^1 > \sigma_3^1$, i.e. with all principal stresses different from each other. The great interest is due to the fact that rock masses and their separate areas are often under this type of stress state. Such stress state is normally observed in the vicinity of underground workings and in the Earth's regions with increased tectonic activity, i.e. exactly where stress measurement is of the highest importance.

So far, no experimental investigations of the Kaiser effect in rock samples, which earlier experienced true triaxial stress state ($\sigma_1^1 > \sigma_2^1 > \sigma_3^1$) with known principal stresses, have been carried out. This is explained through the extreme complexity of such triaxial loading which requires special custom-fabricated equipment. At the same time, the complete absence of any ideas and evaluations on this problem makes a serious handicap to the pratical use of the Kaiser effect for stress measurement in rocks (Shkuratnik et al., 2000).

Some steps in the direction of theoretical investigation of the Kaiser effect under true triaxial state of stress have been undertaken earlier (see Shkuratnik & Lavrov, 1997 b; Lavrov & Yasinskiy, 2000). Simulation of the Kaiser effect in rocks with zero friction ($\mu = 0$, $k = 0$) subjected earlier to triaxial stress state of type $\sigma_1^1 > \sigma_2^1 > \sigma_3^1$ was performed (Shkuratnik & Lavrov, 1997 b). But rocks with zero or near to zero friction are rather uncommon. For most rocks, μ ranges between 0.3 and 0.6 (see e.g. table 1 in Ashby & Sammis (1990)). For such rocks, the simulation results obtained by Shkuratnik & Lavrov (1997) are not valid.
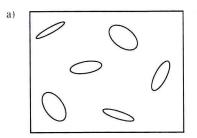
Lavrov & Yasinskiy (2000) have carried out a complete analysis of the behaviour of *one* crack durig two loading cycles, the first of which was true triaxial compression. The second cycle was a conventional uniaxial test. It was shown that the stress value, at which the crack re-starts growing in the second cycle, may strongly depend on the first-cycle intermediate principal stress σ_2^1. From here, one can assume that in rocks containing a large number of arbitrarily oriented cracks the intermediate principal stress should have a strong and complex influence upon the Kaiser effect. This suggestion makes simulate the Kaiser effect in a rock with randomly oriented cracks and non-zero coefficient of friction between crack faces, which previously was under true triaxial stress state. In this article, the simulation procedure and the results obtained are outlined.

2. Theoretical model and simulation procedure

Two loading cycles of a rock sample containing 1000 pre-existing cracks were simulated. The first cycle was proportional true triaxial loading up to the peak values of the principal stresses given by σ_1^1, σ_2^1, and σ_3^1. Here, $\sigma_1^1 > \sigma_2^1 > \sigma_3^1 > 0$, compression is positive, all principal stresses are compressive. After the first cycle had been completed, unloading followed. During unloading, principal stresses were proportionally decreased from $\sigma_1^1, \sigma_2^1, \sigma_3^1$ to zero. Afterwards, the second loading cycle was performed. In the second cycle, the sample was subjected to uniaxial compression. The compression axis in the second cycle coincided with the direction of the first-cycle maximum principal stress σ_1^1.

Prior to the first cycle, all cracks have been of the form of thin penny-shaped flaws. The initial crack radius a and the coefficient of friction between crack faces μ are the same for all cracks. The penny-shaped initial cracks are randomly oriented (Fig. 1 a). The orientation of each crack is defined by three angles $\alpha_i (i = 1, 2, 3)$, at which the normal to the crack plane is inclined to the directions of the first-cycle principal stresses (Fig. 2). The angle α_1 was a random variable uniformly distributed in the range from 0 to $\pi/2$. The angle α_2 was choosen in the same manner as α_1, but the condition $\cos^2\alpha_2 + \cos^2\alpha_1 < 1$ was to be fulfilled. The angle α_3 was then defined automatically from the condition $\sum_i \cos^2 \alpha_i = 1$.

Fig. 1. Rock containing randomly oriented cracks before (*a*) and during (*b*) the first-cycle loading. Initial (pre-existing) penny-shaped cracks and tensile wing cracks are presented in *a* and *b* respectively
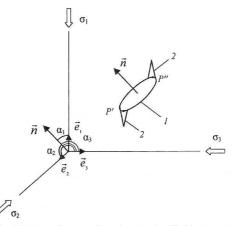
Fig. 2. Penny-shaped crack (*1*) with emerging tensile wing cracks (*2*). Unit vectors, $\vec{e}_i$ indicate the directions of the first-cycle principal stresses. Points P' and P'' on the circular contour of the penny-shaped crack indicate the places where tensile cracks arise. Vector $\vec{n}$ is the normal to the plane of the penny-shaped crack inclined at angles α_i to the principal axes

The solid is presumed not to initially contain any other heterogeneities or discontinuities but penny-shaped cracks. The material containing cracks is homogeneous and isotropic in all mechanical parameters. The cracks are distributed rarely enough to neglect their interaction in both cycles. While the cracks grow, they generate AE pulses. The crack propagation is the only AE source in this model.

The first-cycle loading leads to that a normal stress

$$\sigma_n = \sum_{i=1}^{3} \sigma_i \cos^2 \alpha_i \tag{3}$$

and a shear stress

$$\tau = \left[\sum_{i=1}^{3} (\sigma_i)^2 \cos^2 \alpha_i - \sum_{i=1}^{3} \sum_{j=1}^{3} \sigma_i \sigma_j \cos^2 \alpha_i \cos^2 \alpha_j \right]^{1/2} \tag{4}$$

act over the crack plane. Here, σ_i are current values of the principal stresses. In the course of the first cycle, σ_n and τ increase from zero to the maximum values which can be obtained from expression (3) and (4) substituting σ_i^1 instead of σ_i.

The shear direction over the initial crack plane in the first cycle is defined through the unit vector $\vec{e}_i^1$ which is a function of σ_i^1 and α_i. The effective shear stress in the plane of a penny-shaped initial crack is given by:

$$\tau_{eff} = \tau - \mu \sigma_n \tag{5}$$

when τ is higher than $\mu \sigma_n$; no cohesion between crack faces is implied in this model (Nemat-Nasser & Horii, 1982; Dyskin et al., 1999). If τ is lesser than $\mu \sigma_n$, the value of τ_{eff} is set to be zero.

At each moment, the values of σ_n, τ and τ_{eff} are different for different cracks because of arbitrary crack orientation. The effective stress τ_{eff} reaches its maximum τ_{eff}^I at the end of the first-cycle loading. The value of τ_{eff}^I can be calculated by substituting τ^I and σ_n^I instead of τ and τ_n into equation (5).

Gradual increase of the effective stress in the first cycle results in increasing Mode II and Mode III stress intensity factors on the boundary of the penny-shaped crack. Detailed analysis given by Adams & Sines (1978), Dyskin et al. (1994), Dyskin et al. (1999) has shown that the beginning of the growth of a penny-shaped crack is determined by the Mode II stress intensity factor K_{II}. This growth follows in the form of the generation and propagation of two tensile cracks, the so-called wing cracks (Dyskin et al., 1995; Germanovich et al., 1995). These cracks emerge in two diametrically opposite points P' and P'' of the contour of the penny-shaped crack. Points P' and P'' correspond to the maximum value of K_{II}, which has a cosine dependence on the polar angle (Cherepanov, 1979). The location of the wing initiation points P' and P'' (Fig. 2) is such that the diameter $P'P''$ is parallel to the shear vector $\vec{e}_\tau^I$.

Pressume that the local strength of the matrix material in the vicinity of the penny-shaped crack contour is close to zero. It was shown earlier, for a more simple case of triaxial axisymmetric stress state, that this assumption can only lead to worse results, but does not distort them in essence (Lavrov, 1997 a). Hence, the condition of the tensile crack initiation in the first cycle can be given by

$$\tau_{eff}^I > 0. \tag{6}$$

Condition (6) shows that some of pre-existing penny-shaped cracks do not generate wings in the first cycle, as the shear stress on their planes does not exceed the friction force. Of interest to us are those penny-shaped cracks, which have generated wings in the first cycle, because precisely these cracks are responsible for rock memory about the first-cycle stress state and for the Kaiser effect in the second one.

Tensile cracks appearing in the first cycle have a quite complex spatial shape. They use a part of the circular boundary of the penny-shaped crack as their base (Fig. 2). This base gets larger while the tensile cracks grow (Dyskin et al., 1999). In the cases of uniaxial or axisymmetric triaxial compression, the tensile cracks bend in the way that they get oriented approximately parallel to the direction of the largest compressive principal stress σ_i (see experiments by Adams & Sines (1978), Dyskin et al. (1995), Germanovich et al. (1995)). For true triaxial loading, no experiments of this kind have been carried out. However, we are interested not in the exact shape and orientation of the wings, but only in the criterion of their growth renewal in the second cycle.

The propagation of wings cracks occurs in a stable manner. An increase in τ_{eff} is required for an increase in their length. The Mode I stress intensity factor at the tip of the growing wing crack is given by the difference of two values (Ashby & Sammis, 1990; Dyskin et al., 1999). One of these two terms is directly proportional to the

effective shear stress τ_{eff} and inversely proportional to the wing length l to the power $3/2$, i.e. the first term is proportional to $\tau_{eff}/l^{3/2}$ (Cherepanov, 1979). This dependence on l guarantees that the propagation is stable because the value of K_I decreases with increasing wing length. So an increase in τ_{eff} is required for further crack extension, i.e. for the condition $K_I = K_{Ic}$ to be fulfilled.

The second term in the expression for K_I is directly proportional to the confining stress and to the square root of the wing length $\sqrt{l}$ (see a two-dimensional model developed by Nemat-Nasser & Horii (1982) and three-dimensional models by Costin (1985), Ashby & Sammis (1990), Dyskin et al. (1999) and others). In the case of triaxial axisymmetric loading, the confining stress is presented by $\sigma_2 = \sigma_3$.

In brittle rocks, the Kaiser effect is seen most distinctly at stress values which are relatively far from the failure stress. When approaching the critical damage level, the distinctness of the effect gets worse (see experiments by Li & Nordlund (1993), Panasiyan et al. (2000)). Therefore, we are interested primarily in the initial stage of crack growth, while l is relatively small. At this initial stage, the main contribution to the value of K_I is made by the first term, which is inversely proportional to $l^{3/2}$. Hence, in our model, we can set K_I to be directly proportional to τ_{eff} and inversely proportional to $l^{3/2}$.

$$K_I \propto \tau_{eff}/l^{3/2}. \tag{7}$$

From the crack growth condition $K_I = K_{Ic}$, we conclude that the wing length at the end of the first cycle is proportional to a value as follows:

$$l^I \propto \left(\tau_{eff}^I/K_{Ic}\right)^{2/3}. \tag{8}$$

That is, the length of the tensile cracks after completing the first cycle is defined by the attained value of the effective shear stress τ_{eff}^I.

During the simulation, the values of τ_{eff}^I as well as the vectors $\check{e}_\tau^I$ were computed and memorized for all cracks, which generated wings in the first cycle.

Unloading after the first cycle leads to a mutual backward shear of the faces of penny-shaped cracks. Due to the elasticity of the matrix material and due to the absence of cohesion, the faces of the penny-shaped cracks will return into their initial position after being completely unloaded. This position is the same as it was before the first cycle. Tensile cracks will close after unloading.

During uniaxial reloading in the second cyle in the direction of σ_1 of the first cycle, the normal stress

$$\sigma_n = \sigma_1 \cos^2\alpha_1 \tag{9}$$

and the shear stress

$$\tau = \frac{\sigma_1}{2}\sin 2\alpha_1 \tag{10}$$

are acting in the plane of each penny-shaped crack. The effective shear stress is given by expression (5) when τ is higher than $\mu\sigma_n$. When τ is lesser than $\mu\sigma_n$, τ_{eff} is set to be zero. The unit shear vector $\vec{e}_\tau^{II}$ in the second cycle is given by

$$\vec{e}_\tau^{II} = \vec{e}_1 \sin\alpha_1 - \vec{e}_2 \operatorname{ctg}\alpha_1 \cos\alpha_2 - \vec{e}_3 \operatorname{ctg}\alpha_1 \cos\alpha_3, \qquad (11)$$

where $\vec{e}_i (i = 1, 2, 3)$ are unit vectors in the directions of the first-cycle principal stresses (Fig. 2).

There are several opportunities for crack behaviour in the second cycle depending on whether the penny-shaped crack generated wings in the first cycle as well as on the mutual orientation of the shear vectors in the first and second cycles, $\vec{e}_\tau^I$ and $\vec{e}_\tau^{II}$. Consider theses alternatives.

1. The penny-shaped crack did not generate tensile cracks (wings) in the first cycle. The condition (6) was not fulfilled.

In this case, the penny-shaped crack will generate tensile cracks in the second cycle if condition (6) is fulfilled. The value of σ_1, at which wings emerge in the second cycle, is not connected with the stress state experienced in the first one. Such cracks do not contribute to the formation of the Kaiser effect in the second cycle. AE from this type of cracks is a noise and makes it difficult to recognize the Kaiser effect reliably.

2. The penny-shaped crack did generate tensile cracks (wings) in the first cycle. The condition (6) was fulfilled.

Two sub-types of behaviour of such cracks are possible in the second cycle, depending on the sign of the scalar product of the shear vectors in the first and second cycles $(\vec{e}_\tau^I \cdot \vec{e}_\tau^{II})$ (Lavrov, 1997 a; Lavrov & Yasinski, 2000).

2 a. $(\vec{e}_\tau^I \cdot \vec{e}_\tau^{II}) < 0$

In this case, both tensile cracks generated in the first cycle should close in the second one, because the projection of the second-cycle shear vector $\vec{e}_\tau^{II}$ onto the first-cycle shear vector $\vec{e}_\tau^I$ is negative. Calculation shows that it is possible only if the condition

$$(\sigma_1^I - \sigma_2^I)\cos^2\alpha_2 + (\sigma_1^I - \sigma_3^I)\cos^2\alpha_3 < 0 \qquad (12)$$

is fulfilled. Since all σ_i^I are positive and are chosen in the way that $\sigma_1^I > \sigma_2^I > \sigma_3^I$, there are no cracks for which condition (12) is satisfied. Hence, case 2 a is not realizable in our task.

2 b. $(\vec{e}_\tau^I \cdot \vec{e}_\tau^{II}) > 0$.

In that event, the second-cycle shear vector has a positive component in the direction of the first-cycle shear vector. Therefore, tensile cracks generated in the first cycle will open again in the second one and will re-start growing

at a certain stress value σ_{1*}^{II}. The condition of the propagation onset for these cracks in the second cycle is given by

$$\tau_{eff} \cdot (\dot{e}_\tau^I \cdot \dot{e}_\tau^{II}) \geqslant \tau_{eff}^I. \tag{13}$$

Here, τ_{eff} is the current value of the effective stress in the second cycle. After some little algebra, obtain that the value of the uniaxial compressive stress at which a crack re-starts growing in the second cycle is given by

$$\sigma_{1*}^{II} = \frac{\left(\tau^I - \mu \sum_{i=1}^{3} \sigma_i^I \cos^2 \alpha_i\right) \tau^I}{\cos\alpha_1 \operatorname{ctg}\alpha_1 \left(\sin\alpha_1 - \mu\cos\alpha_1\right)\left(1 - \sum_{i=1}^{3} \cos^2 \alpha_i\right)}. \tag{14}$$

The fact that a crack renews its growth means that acoustic emission pulses are generated by this crack again. The cracks of type 2 b are responsible for Kaiser effect in the second cycle.
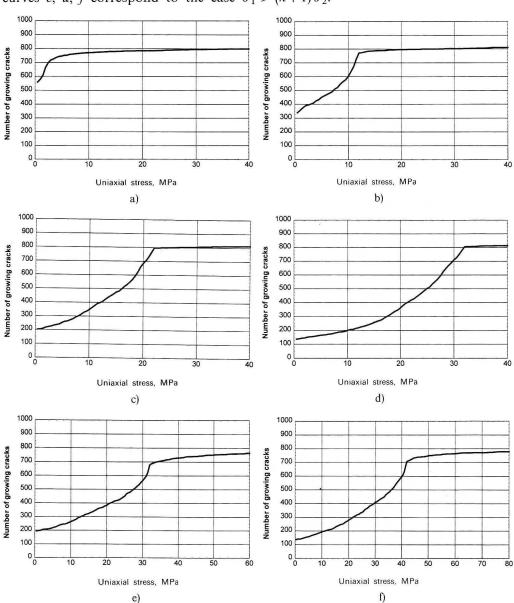
According to (14), the value of σ_{1*}^{II} is a function of $\alpha_i (i = 1, 2, 3)$. As a result, in a rock with random initial crack orientation, all cracks re-start to grow at different stress values in the second cycle. The Kaiser effect takes place in the second cycle, but its form is essentially more complex than that in the case of uniaxial compression in both cycles.

In our computer experiments, the second loading cycle was performed in steps. The value of σ_1 was increased by equal increments, usually by 1 MPa. At each stress step the growth conditions were checked for each crack, i.e. condition (6) for type 1 cracks and condition (13), $\sigma_1 \geqslant \sigma_{1*}^{II}$, for cracks of type 2 b. The total number N of cracks growing at this stress value was computed. This number N was adopted to be a measure of AE activity at this stress level. A similar approach was succesfully used earlier when simulating the Kaiser effect in rocks around a borehole (Lavrov, 1997 b; Chkouratnik & Lavrov, 1997; Lavrov, 1998) as well as in rock samples subjected to uniaxial or axisymmetric traxial compression in both cycles (Lavrov, 1997 a; Shkuratnik & Lavrov, 1998; Lavrov, 2000). The value of N allows to qualitatively judge the intensity of crack growth processes during loading of rock.

According to computation results, graphs "number of growing cracks N versus uniaxial stress σ_1" were plotted for the second cycle.

3. Simulation results and their discussion

A series of computer experiments was conducted for various combinations of the first-cycle principal stresses σ_1^I, σ_2^I, σ_3^I and for rocks with various values of the coefficient of friction μ. As an example, some graphs for rocks with $\mu = 0.3$ and $\mu = 0.6$ are depicted in Figures 3 and 4 respectively. The interrelations between σ_1^I, σ_2^I, and σ_3^I for curves in Figures 3 and 4 are as follows (cf. expression for the threshold memorizable stress value: $\sigma_1^I - (k+1)\sigma_{2,3}^I$).

In Fig. 3 $\mu = 0.3$, $k = 0.806$, curve a corresponds to the case $(k+1)$ $\sigma_3^I \cong \sigma_1^I < (k+1)\sigma_2^I$; curves b, e correspond to the case $(k+1)\sigma_3^I < \sigma_1^I < (k+1)\sigma_2^I$; curves c, d, f correspond to the case $\sigma_1^I > (k+1)\sigma_2^I$.

Fig. 3. Curves "Number of growing cracks versus stress σ_1" plotted for uniaxial loading of rock samples which previously (*in situ*) were under triaxial stress states with various principal stress combinations: $a - \sigma_1^I = \sigma_2^I = 20$ MPa, $\sigma_3^I = 10$ MPa; $b - \sigma_1^I = 30$ MPa, $\sigma_2^I = 20$ MPa, $\sigma_3^I = 10$ MPa; $c - \sigma_1^I = 40$ MPa, $\sigma_2^I = 20$ MPa, $\sigma_3^I = 10$ MPa; $d - \sigma_1^I = 50$ MPa, $\sigma_2^I = 20$ MPa, $\sigma_3^I = 10$ MPa; $e - \sigma_1^I = 50$ MPa, $\sigma_2^I = 30$ MPa, $\sigma_3^I = 10$ MPa; $f - \sigma_1^I = 60$ MPa, $\sigma_2^I = 30$ MPa, $\sigma_3^I = 10$ MPa $\mu = 0.3$, $k = 0.806$ for all curves

In Fig. 4 $\mu = 0.6$, $k = 2.12$, curve a corresponds to the case $\sigma_1^I < (k+1)\sigma_3^I$, $\sigma_1^I < (k+1)\sigma_2^I$; curve b corresponds to the case $(k+1)\sigma_3^I < \sigma_1^I < (k+1)\sigma_2^I$; curve c corresponds to the case $(k+1)\sigma_3^I < \sigma_1^I \cong (k+1)\sigma_2^I$; curves d, e and f correspond to the case $\sigma_1^I > (k+1)\sigma_2^I$, $\sigma_1^I > (k+1)\sigma_3^I$.
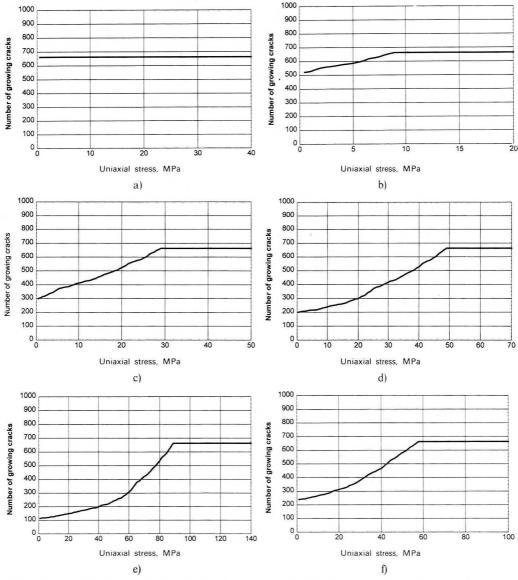

Fig. 4. Curves "Number of growing cracks versus stress σ_1" plotted for uniaxial loading of rock samples which previously (*in situ*) were under triaxial stress states with various principal stress combinations: $a - \sigma_1^I = 25$ MPa, $\sigma_2^I = 20$ MPa; $\sigma_3^I = 10$ MPa; $b - \sigma_1^I = 40$ MPa, $\sigma_2^I = 20$ MPa, $\sigma_3^I = 10$ MPa; $c - \sigma_1^I = 60$ MPa, $\sigma_2^I = 20$ MPa, $\sigma_3^I = 10$ MPa; $d - \sigma_1^I = 80$ MPa, $\sigma_2^I = 20$ MPa, $\sigma_3^I = 10$ MPa; $e - \sigma_1^I = 120$ MPa, $\sigma_2^I = 20$ MPa, $\sigma_3^I = 10$ MPa; $f - \sigma_1^I = 120$ MPa, $\sigma_2^I = 30$ MPa, $\sigma_3^I = 20$ MPa $\mu = 0.6$, $k = 2.12$ for all curves

Kaiser effect manifests itself as an inflexion in curve "number of growing cracks versus stress". In Fig. 3 b, c, d these inflexions are seen at $\sigma_1 \cong 12$, 22, and 32 MPa respectively. In Fig. 4 b, c, d, e the inflexions are located at 9, 29, 49, and 89 MPa respectively.

Such interpretation of the simulation curves was adopted earlier while simulating the case of axisymmetric first-cycle loading (Lavrov, 1997 a) and demonstrated a good agreement with experiment (Filimonov et al., 2000 a; Li & Nordlund, 1993).

Analysis of curves obtained for various combinations of the first-cycle principal stresses shows that increasing σ_1^I by 10 MPa when σ_2^I and σ_3^I remain constant results in increase of the Kaiser effect stress by 10 MPa as well. This means that the Kaiser effect can help evaluate the largest principal stress values for *in situ* stress conditions with similar σ_2^I, σ_3^I and μ but different σ_1^I.

Curve "Number of growing cracks versus stress" for uniaxial compression of a rock which was previously (*in situ*) subjected to true triaxial stress state $\left(\sigma_1^I > \sigma_2^I > \sigma_3^I\right)$ is located between two curves corresponding to extreme cases with $\sigma_1^I > \sigma_2^I = \sigma_2^I$ and $\sigma_1^I > \sigma_3^I = \sigma_3^I$ (Fig. 5). The Kaiser effect in rock samples subjected earlier to true triaxial stress state manifests itself lesser distinctly than that in the samples pre-loaded in axisymmetric triaxial compression of type $\sigma_1^I > \sigma_2^I = \sigma_2^I$ or $\sigma_1^I > \sigma_3^I = \sigma_3^I$. In a uniaxial test of a sample, which experienced earlier true triaxial stress state, AE activity increases in a more-or-less stable fashion in the stress range from $\sigma_1 = 0$ to $\sigma_{1EK}^I = \sigma_1^I - (k+1)\sigma_2^I$, where k is a dimensionless coefficient defined by exp. (2). E.g., in Fig. 5 $\sigma_{1EK}^{II} = 50$ MPa.

In rock samples which were subjected to axisymmetric triaxial stress state in the first cycle, the Kaiser effect takes the form of a sharp increase in AE activity occurring when σ_1 approaches the value of σ_{1EK}^{II} (20 MPa for dotted line and 50 MPa
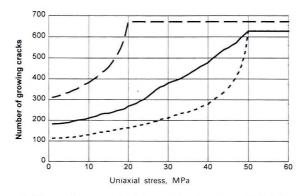

Fig. 5. The dependence of AE activity on uniaxial compressive stress (MPa) for uniaxial tests of rock samples which were previously (*in situ*) subjected to triaxial compression. The *in situ* stress state was true triaxial compression with $\sigma_1^I = 80$ MPa, $\sigma_1^I = 20$ MPa, $\sigma_3^I = 10$ MPa (solid line), triaxial axisymmetric compression with $\sigma_1^I = 80$ MPa, $\sigma_2^I = \sigma_3^I = 20$ MPa (dotted line) and triaxial axisymmetric compression with $\sigma_1^I = 80$ MPa, $\sigma_2^I = \sigma_3^I = 10$ MPa (point line). The coefficient of friction between crack faces $\mu = 0.58$ for all three curves

for point line in Fig. 5). For rocks which were loaded by true triaxial stress state *in situ* (solid line in Fig. 5), no dramatic increase in AE activity is observed. This circumstance makes it difficult to recognize and to interpret the Kaiser effect in such samples.

The shape of the dotted and pointed curves in Fig. 5 is in general very similar to real curves obtained in laboratory tests on rock samples previously subjected to triaxial axisymmetric loading with $\sigma_1^I > \sigma_{1th}^I$. This allows to expect that the shape of the simulation curve for a sample earlier experienced true triaxial stress state is not far from reality too.

Laboratory experiments show that, after the stress has reached σ_{1EK}^{II}, AE activity begins to decrease gradually (Filimonov et al., 2000 a), i.e. the Kaiser effect has the form of a maximum in curve "Number of growing cracks versus stress", taking place at $\sigma_1 = \sigma_{1EK}^{II}$. The decrease in AE activity which has been observed in the samples subjected to triaxial axisymmetric loading in the first cycle, is due to the interaction and coalescence of growing cracks. Such interaction processes can lead to complete arrest of cracks involving the arrest of AE generated by them (see e.g. Eberhardt et al., 1998).

Computer experiments have shown that AE activity in a sample experienced *in situ* true triaxial stress state $\sigma_1^I > \sigma_2^I > \sigma_3^I$ attains its maximum at the same stress value as that of the sample experienced axisymmetric triaxial stress state of type $\sigma_1^I > \sigma_3^I = \sigma_3^I$ (Fig. 5). However, the background AE activity at lower stress values (i.e. at $\sigma_1 = \sigma_{1EK}^{II}$) in a sample after true triaxial loading is higher than that in a sample after axisymmetric one ($\sigma_1^I > \sigma_3^I = \sigma_3^I$).

In general, it can not be concluded from the shape of curves "Number of growing cracks versus stress" only, whether the *in situ* stress state of rock was axisymmetric or true triaxial. At best, the presence of the Kaiser effect indicates that the relation

$$\sigma_1^I > (k+1)\sigma_3^I \tag{15}$$

was fulfilled *in situ*. In this case, the Kaiser effect stress allows to estimate the value of linear combination of *in situ* principal stresses given by $\sigma_1^I - (k+1)\sigma_3^I$. For this purpose, the value of k can be easily found through laboratory triaxial tests of the rock in question as it is considered by Holcomb (1983) and Li (1998). To evaluate absolute values of the *in situ* principal stresses, it is necessary to perform some other, more sophisticated experiments as it was proposed e.g. by Shkuratnik & Lavrov (1998)).

The nature of the Kaiser effect in rocks which were previously loaded in true traxial stress state depends on the coefficient of friction between crack faces μ. Curves "Number of growing cracks versus stress" for rock samples pre-loaded with true triaxial stress state and for those pre-loaded with axisymmetric triaxial stress state are located closer to each other in rocks with lower friction.

The results obtained are of great interest for development of stress measurement methods on the basis of the Kaiser effect. Unfortunately, modern applications of the

Kaiser effect in core samples for stress estimation either do not take triaxial nature of the *in situ* stress state into account at all (Nag et al., 1996; Kuwahara et al., 1990; Kanagawa & Nakasa, 1978) or suppose the *in situ* stress state to be exisymmetric (Holcomb & Martin, 1985). However, our simulation has shown that the Kaiser effect is strongly influenced by both, the second and third principal stresses. They both lead to a change in the Kaiser effect manifestation and to a reduction of the stress at which the effect takes place. As an example, simulation curves "Number of growing cracks versus stress" are depicted in Fig. 6 for several rocks that were *in situ* subjected to various stress states: uniaxial, triaxial axisymmetric and true triaxial. The value of the maximum principal stress, σ_1^1 is the same for all curves. The only difference between the curves is in the values of σ_2^1 and σ_3^1. It is clearly seen from Fig. 6 that the curve shape and the Kaiser effect stress value are essentially dependent on both intermediate σ_2^1 and minimum σ_3^1 principal stresss. Not taking the influence of σ_3^1 and σ_2^1 into account can lead to misinterpreting of stress measurement data.
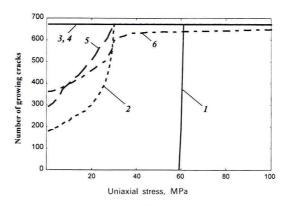

Fig. 6. The dependence of AE activity on uniaxial compressive stress (MPa) for uniaxial tests of six rock samples which were previously (in situ) subjected to triaxial stress state with the same largest principal stress $\sigma_1^1 = 60$ MPa for all samples but different combinations of the second and third principal stresses: $1 - \sigma_2^1 = \sigma_3^1 = 0$; $2 - \sigma_2^1 = \sigma_3^1 = 10$ MPa; $3 - \sigma_2^1 = \sigma_3^1 = 40$ MPa; $4 - \sigma_2^1 = \sigma_3^1 = 60$ MPa; $5 - \sigma_2^1 = 20$ MPa; $\sigma_3^1 = 10$ MPa; $6 - \sigma_2^1 = 40$ MPa, $\sigma_3^1 = 10$ MPa. The coefficient of friction between crack faces $\mu = 0.58$ for all curves.

4. Conclusions

Numerical simulation has shown that the Kaiser effect manifestation in rock samples, pre-loaded with true triaxial stress state in situ ($\sigma_1^1 > \sigma_2^1 > \sigma_3^1$), is essentially more complex than in the samples, pre-loaded with axisymmetric stress state of type $\sigma_1^1 > \sigma_2^1 = \sigma_2^1$ or $\sigma_1^1 > \sigma_3^1 = \sigma_3^1$. The curve "AE activity versus stress" does not exhibit any sharp increase in AE activity; AE begins to grow just from the beginning of the uniaxial laboratory loading and gradually increases, until its maximum is reached at $\sigma_1 = \sigma_1^1 - (k+1)\sigma_3^1$. Here, k is a dimensionless coefficient specific for the rock. The

distinction of the Kaiser effect in uniaxial tests of rocks which were under true triaxial stress state *in situ* is worse than this is in rocks which were under triaxial axisymmetric stress state *in situ*. Using only the curve "AE activity versus stress" obtained in a uniaxial compressive test of a core sample, it is hardly possible to recognize the type of the *in situ* stress state. It is impossible to estimate absolute values of the *in situ* principal stresses as well. The second and the third *in situ* principal stresses σ_2^1 and σ_3^1 have a pronounced influence on the Kaiser effect stress in extracted core samples. The nature of the Kaiser effect and the degree of influence of the intermediate *in situ* principal stress σ_2^1 are functions of the coefficient of friction between crack faces.

REFERENCES

A d a m s M., S i n e s G., 1978. Crack extension from flaws in a brittle material subjected to compression. Tectonophysics **49**, 1/2, 97–118.

A s h b y M. F., S a m m i s C. G., 1990. The damage mechanics of brittle solids in compression. Pure and Applied Geophysics (PAGEOPH) **133**, 3, 489–521.

C h e r e p a n o v G. P., 1979. Mechanics of Brittle Fracture. McGraw Hill, New York.

C h k o u r a t n i k V. L., L a v r o v A. V., 1997. Numerical 2D-simulation of memory effects in rocks around a borehole. Proc. International Symposium on Rock Stress, Kumamoto, Japan, 7–10 October. Rotterdam: A. A. Balkema, 193–196.

C o s t i n L. S,, 1985. Damage mechanics in post-failure regime. Mechanics of Materials **4**, 2, 149–160.

D y s k i n A. V., G e r m a n o v i c h L. N., J e w e l l R. J., J o e r H., K r a s i n s k i J. S., L e e K. K., R o e g i e r s J.-C., S a h o u r y e h E., U s t i n o v K. B., 1995. Some experimental results on three-dimensional crack propagation in compression. Proc. 2nd International Conference on Mechanics of Jointed and Faulted Rock (MJFR-2), Vienna, Austria, 10–14 April. Rotterdam: A. A. Balkema, 91–96.

D y s k i n A. V., G e r m a n o v i c h L. N., U s t i n o v K. B., 1999. A 3-D model of wing crack growth and interaction. Engineering Fracture Mechanics **63**, 1, 81–110.

D y s k i n A. V., J e w e l l R. J., J o e r H., S a h o u r y e h E., U s t i n o v K. B., 1994. Experiments on 3-D crack growth in uniaxial compression. International Journal of Fracture **65**, 4, R77-R83.

E b e r h a r d t E., S t e a d D., S t i m p s o n B., L a j t a i E. Z., 1998. The effect of neighbouring cracks on elliptical crack initiation and propagation in uniaxial and traxial stress fields. Engineering Fracture Mechanics **59**, 2, 103–115.

F i l i m o n o v Yu. L., L a v r o v A. V., S h a f a r e n k o Ye. M., S h k u r a t n i k V. L., 2000 a. Memory effects in rock salt under triaxial stress state and their use for stress measurement in a rock mase (in preparation).

F i l i m o n o v Yu. L., L a v r o v A. V., S h a f a r e n k o Ye. M., S h k u r a t n i k V. L., 2000 b. Experimentelle Untersuchung des Steinsalzes mittels einaxialem Drucktest mit hydrostatischer Vorbelastung. Glückauf-Forschungshefte, **61**, 2 (in German; in press).

G e r m a n o v i c h L. N., R i n g L. M., C a r t e r B. J., I n g r a f f e a A. R., D y s k i n A. V., U s t i n o v K. B., 1995. Simulation of crack growth and interaction in compression. Proc. 8th International

Congress on Rock Mechanics, Tokyo, Japan, 25–30 September. Rotterdam: A. A. Balkema, vol. 1, 219–226.

H o l c o m b D. J., 1983. Using acoustic emissions to determine in situ stress: problems and promise. Proc. Applied Mechanics, Bioengineering and Fluids Engineering Conference, Houston, USA, 11–21.

H o l c o m b D. J., M a r t i n R. J. III, 1985. Determining peak stress history using acoustic emissions. Proc. 26th US Symposium on Rock Mechanics, Rapid City, USA, 26–28 June. Rotterdam: A. A. Balkema, vol. 2, 715–722.

H u g h s o n D. R., C r a w f o r d A. M., 1987. Kaiser effect gauging: The influence of confining stress on its response. Proc. 6th International Congress on Rock Mechanics, Montreal, Canada. Rotterdam: A. A. Balkema, vol. 2, 981–985.

K a i s e r J., 1953. Erkenntnisse und Folgerungen aus der Messung von Geräuschen bei Zugbeanspruchung von metallischen Werkstoffen. Archiv für das Eisenhüttenwesen **24**, 1/2, 43–45.

K a n a g a w a T., N a k a s a H., 1978. Method of estimating ground pressure. U. S. Patent No. 4107981.

K u r i t a K., F u j i i N., 1979. Stress memory of crystalline rocks in acoustic emission. Geophysical Research Letters **6**, 1, 9–12.

K u w a h a r a Y., Y a m a m o t o K., H i r a s a w a T., 1990. An experimental and theoretical study of inelastic deformation of brittle rocks under cyclic uniaxial loading. Tohoku Geophysical Journal (Sci. Rep. Tohoku Univ., Ser. 5: Geophysics) **33**, 1, 1–21.

L a v r o v A. V., 1997 a. Three-dimensional simulation of memory effects in rock samples. Proc. International Symposium on Rock Stress, Kumamoto, Japan, 7–10 October. Rotterdam: A. A. Balkema, 197–202.

L a v r o v A. V., 1997 b. Computer simulation of memory relaxation in rocks around a borehole. Archives of Mining Sciences (Archiwum Górnictwa) **42**, 3, 353–365.

L a v r o v A. V., 1998. Development of theoretical models of emission memory effects in rocks. Ph. D. thesis, Moscow State Mining University, Russia (in Russian).

L a v r o v A. V., 2000. Features of AE kinetics simulation in cyclically loaded rocks. Geoecology and Computers. Pric. 3rd International Conference on Advances of Computer Methods in Geotechnical and Geoenvironmental Engineering, Moscow, Russia, 1–4 February. Rotterdam: A. A. Balkena, 407–410.

L a v r o v A. V., Y a s i n s k i M. V., 2000. On the influence of intermediate principal stress upon acoustic emission in cyclically loaded rocks. Proc. of the 10th Session of the Russian Acoustical Society, Moscow, Russia, 23–26 May, 211–214 (in Russian; extended abstract in English in Internet at URL: http://www.akin.ru/e_main.htm).

L i C., 1998. A theory for the Kaiser effect and its potential applications. Proc. 6th Conference on AE/MA in Geologic Structures and Materials. Clausthal-Zellerfeld, Trans. Tech. Publ., 171–185.

L i C., N o r d l u n d E., 1993. Experimental verification of the Kaiser effect in rocks. Rock Mechanics and Rock Engineering **26**, 4, 333–351.

N a g D. K., S e t o M., V u t u k u r i V. S., 1996. Application of acoustic emission technique in estimating in situ vertical stress from borehole core rock sample. Trends in NDE Science & Technology. Proc. 14th World Conference on Non-Destructive Testing, New Delhi, India, 8–13 December. Ashgate Publishing Comp., vol. 4, 2447–2450.

N e m a t - N a s s e r S., H o r i i H., 1982. Compression-induced nonplanar crack extension with application to splitting, exfoliation, and rockburst. Journal of Geophysical Research **87**, B8, 6805–6821.

P a n a s i y a n L. L., L a v r o v A. V., M a s t y u k o v A. G., 2000. On the felicity ratio of acoustic emission memory effect in several types of rocks. Vestnik MGU (Bulletin of the Moscow State M. V. Lomonosov-University). Ser. 4. Geology (accepted for publication; in Russian).

P i n i ń s k a J., Z u b e r e k W. M., 1998. Effects of discrete memory during rock deformation. Proc. 3rd International Conference on Mechanics of Jointed and Faulted Rock (MJFR-3), Vienna, Austria, 6–9 April. Rotterdam: A. A. Balkema, 393–399.

R z h e v s k i V. V., Y a m s h c h i k o v V. S., S h k u r a t n i k V. L., L y k o v K. G., 1983. Emission memory effects in rocks. Doklady AN SSSR **273**, 5, 1094–1097 (in Russian).

S h k u r a t n i k V. L., L a v r o v A. V., 1995. Memory effects in rock. Journal of Mining Science (Plenum Publ. Corp.) **31,** 1, 20 – 28.

S h k u r a t n i k V. L., L a v r o v A. V., 1997 a. Memory effects in rocks: physical features and theoretical models. Moscow: Academy of Mining Sciences Press (in Russian).

S h k u r a t n i k V. L., L a v r o v A. V., 1997 b. Dreidimensionale Computersimulation des Kaiser-Effektes von Gesteinsproben bei triaxialer Belastung. Glückauf-Forschungshefte **58,** 2, 78 – 81 (in German).

S h k u r a t n i k V. L., L a v r o v A. V., 1998. Numerical simulation of the Kaiser effect under triaxial stress state. Proc. 3rd International Conference on Mechanics of Jointed and Faulted Rock (MJFR-3), Vienna, Austria, 6 – 9 April. Rotterdam: A. A. Balkema, 381 – 385.

S h k u r a t n i k V. L., L a v r o v A. V., K o l o d i n a I. V., 2000. Kaiser-Effekt in Gesteinen und Gebirgsspannungsmeßverfahren auf dessen Grundlage. Proc. EUROCK'2000 Symposium, Aachen, Germany, 27 – 31 March. Essen: Verlag Glückauf, 543 – 548 (in German).

Y o s h i k a w a S., M o g i K., 1981. A new method for estimation of the crustal stress from cored rock samples: laboratory study in the case of uniaxial compression. Tectonophysics **74,** 3/4, 323 – 339.